J Therm Anal Calorim (2012) 107:463–469
DOI 10.1007/s10973-011-1685-4

Particle size effects on the thermal behavior of hematite

Monica Sorescu · Tianhong Xu

Received: 3 January 2011 / Accepted: 19 May 2011 / Published online: 3 June 2011

Abstract Hematite with different particle sizes was obtained through isothermal annealing and mechano-chemical ball-milling methods. The hematite phase is very stable under air atmosphere. The thermal stabilities of hematite under argon atmosphere were characterized by thermal analysis studies up to 800 °C using a simultaneous DSC–TG technique. The lattice parameters *a* and *c* of hematite with different particle sizes were extracted from the Rietveld structural refinement of powder X-ray diffraction patterns. Decomposition of hematite into a lower oxidation state in inert argon atmosphere was studied by the TG experiments for the first time and the enthalpy associated with the decomposition reaction was determined from the DSC studies. Particle size has a strong effect on the thermal behavior of hematite samples. Ball-milled hematite samples with smaller particle size showed that the phase transformation was extended to higher temperature range with larger enthalpy. Hematite with larger average particle size showed higher stability under argon atmosphere.

Keywords Hematite · X-ray diffraction · Simultaneous DSC–TG · Phase transformation · Ball milling

Introduction

Iron oxides play an important role in industry, such as semiconductive compounds, inorganic pigments, magnetic tapes, catalysis, and gas sensing [1–5]. The structure of most iron oxides can be described in terms of closed packed planes of oxygen atoms with iron occupying the interstitial octahedral and tetrahedral sites. The stacking of the closed packed oxygen planes can be hexagonal or cubic. In most cases, both hexagonal and cubic polymorphs exist [6].

Hematite, α-Fe_2O_3, is the most stable and abundant iron oxide, in which the close packed planes of oxygen atoms are stacked in a hexagonal (ABAB…) structure, with iron (III) ions occupying octahedral sites. Magnetite, Fe_3O_4, with the cubic oxygen arrangement (ABCABC…) belongs to the spinel group of minerals [7]. Magnetite can be converted to hematite under progressive oxidation. Fe^{2+} in magnetite is converted to Fe^{3+} until the composition of Fe_2O_3 is reached [8]. It is also well known that hematite can be reduced to magnetite under reduction atmosphere conditions. Wüstite, FeO, is another mineral form of iron (II) oxides. Wüstite crystallizes in the isometric-hexoctahedral crystal system. While the great variety of structures of iron oxides has been recognized, the difference in thermal stability of these oxides under high temperature in argon and dry air atmosphere is not well known. The thermal stability of higher oxidation states of Fe(VI) has been studied under oxygen stream in the temperature range of 200–1000 °C. The formation of pentavalent K_3FeO_4 and trivalent $KFeO_2$ as thermal decomposition products of K_2FeO_4 was observed [9, 10]. There are literature discrepancies in the results regarding the possible formation of intermediate oxidation state of iron, Fe(V) and Fe(IV) as well as final oxide phases, which have not been fully characterized in the thermal decomposition of K_2FeO_4 and $BaFeO_4$ [11]. Recently, surface science characterization techniques were widely used to study the formation and transformation of iron oxides. These studies provided information on structural changes occurring during

M. Sorescu (✉) · T. Xu
Department of Physics, Duquesne University, 211 Bayer Center, Pittsburgh, PA 15282-0321, USA
e-mail: sorescu@duq.edu

oxidation or reduction of iron oxide surfaces. Partial reduction of hematite to magnetite forms α-Fe_2O_3/Fe_3O_4 interface structures which have been observed using high-resolution transmission electron microscopy and multiple orientation relationships between magnetite and hematite have been observed [12–14].

Understanding the thermodynamic properties of the transformation between hematite, magnetite, and wüstite finds application in the characterization of numerous catalytic processes [15–17]. Several studies of transformation among these phases are mainly focused on the oxidation of wüstite to magnetite or hematite, and from magnetite to hematite [18, 19], or with special reference to magnetic properties, but not in terms of the decomposition of hematite to magnetite or magnetite to wüstite. Recently, it was also reported that the particle size of hematite has a strong effect on the thermal behavior of rutile and anatase-doped hematite ceramic systems, and the additions of rutile and anatase suppressed the crystallization of hematite [20, 21]. The hematite with smaller particle sizes showed higher heat capacity due to the presence of water on the surface [22]. Thus, the aim of this study is to measure the thermal behavior of hematite with different particle sizes. Therefore, it is important to understand the thermogravimetric behaviors of hematite (α-Fe_2O_3) in different types of atmospheres, such as air and inert gas atmospheres.

These investigations were aimed at fabricating hematite samples with different particle sizes through isothermal annealing and mechanochemical activation by the ball-milling method. The effect of particle sizes on the thermal behavior was investigated by means of simultaneous DSC–TG measurements in argon atmosphere up to 800 °C. The thermal stability of hematite in dry air atmosphere was tested by annealing at different temperatures. The phases were identified by using powder X-ray diffraction measurements. Particle sizes were estimated using Scherrer equation and lattice parameters were extracted from Rietveld structural refinement of XRD patterns.

Experimental

The precursors of hematite were obtained from Alfa Aesar: hematite (α-phase, 99% metals basis). To obtain the hematite samples with bigger particle size, samples were isothermally annealed in air for 1 h at 450, 550, 650, and 750 °C, respectively, by using a rapid temperature furnace. Mechanochemical activation through ball-milling method was applied to obtain hematite samples with smaller particle sizes [23].

Simultaneous DSC and TG experiments were performed using a Netzsch Model STA 449 F3 Jupiter instrument with a silicon carbide (SiC) furnace. Samples were contained in a manufacturer's alumina crucible with an alumina lid. Series of experiments were performed using 12 ± 1 mg sample size. The atmosphere was flowing protective argon gas at a rate of 50 mL/min. DSC and TG curves were obtained by heating samples from room temperature to 800 °C with a ramp rate of 10 °C/min. Both DSC and TG curves were corrected by subtraction of baselines which was run under identical conditions as the DSC–TG measurements with residue of samples in the crucible. The Netzsch Proteus Thermal Analysis software was used for DSC and TG data analysis.

The X-ray powder diffraction patterns of samples were obtained using an automatic PANalytic X'Pert Pro diffractometer with CuK_α radiation (45 kV/40 mA, $\lambda = 1.5406$ Å) with a nickel filter on the diffracted side. A silicon-strip detector called X'cellerator was used. The scanning range was 10–80° (2θ) with a step size of 0.02°. The identification of crystalline phases was accomplished by comparison with JCPDS files for hematite and magnetite, respectively, and was reported after Rietveld structural refinement.

Results and discussion

The DSC curve of the original hematite sample showed an exothermic peak at 358 °C. Another exothermic peak starts at 600 °C and is not completed in the studied temperature range (Fig. 1a). The existence of double peaks in the DSC curve indicates that hematite is not stable under high temperature and argon atmosphere. Even if the second peak is not completed, the DSC curve of hematite indicates a two-step mechanism of phase change. The first phase change is completed below 600 °C with a peak value at 358 °C, while the second phase change starts at 600 °C. These two phase changes are entirely separated, which indicates that the second phase change occurs after the first phase change is completed. Integration of the first peak gives an enthalpy value of 1.16 kJ/g. No exact enthalpy value can be extracted for the second phase change since the second phase transition is not completed in the temperature range investigated.

The mass losses of the original hematite samples were investigated using TG analysis. As can be seen in Fig. 1f, the thermogravimetry reveals two major mass losses for the original hematite sample: one is in a relatively low temperature range from 100 to 600 °C, and the other starts above 600 °C. These two mass losses are due to the decomposition of hematite. The primary mass loss is possibly related to the decomposition of hematite to magnetite (or a less stoichiometric hematite), as shown in Eq. 1. The secondary mass loss at above 650 °C is mainly possibly

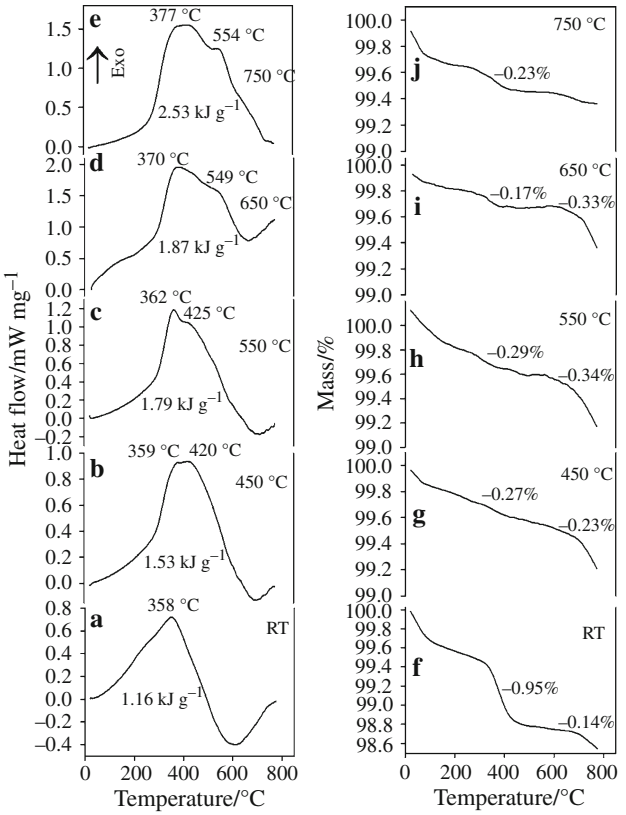

Fig. 1 DSC curves of hematite samples annealed at *a* room temperature, *b* 450 °C, *c* 550 °C, *d* 650 °C, *e* 750 °C, and TG curves of hematite samples annealed at *f* room temperature, *g* 450 °C, *h* 550 °C, *i* 650 °C, *j* 750 °C

caused by the further decomposition of magnetite to wüstite, as shown in Eq. 2.

$$3Fe_2O_3 \rightarrow 2Fe_3O_4 + 1/2O_2 \quad (1)$$

$$Fe_3O_4 \rightarrow 3FeO + 1/2O_2. \quad (2)$$

These two mass losses are in good agreement with the DSC curves of the original hematite (Fig. 1a), which show one exothermic peak, with a sign of second peak beginning to develop above 600 °C. The first phase change in DSC curve with a broad peak below 600 °C corresponds to the first mass loss, and the peak temperature of 358 °C is exactly at the centre of the TG curve where the first mass loss occurs. It has been reported that hematite completely decomposes to magnetite in the presence of high boiling point solvent 1-octadecence under N_2 atmosphere at 320 °C for 28 h refluxing [24], such that this temperature is in the temperature range of the first DSC exothermic peak. The mass loss occurred in a relatively small temperature range comparing to the broad temperature range of the DSC curve. This also indicates that the mass loss occurs simultaneously with the crystallization of fine hematite particles. The second mass loss starts around 700 °C and the DSC curve shows a rising value of the heat flow although this peak is not completed in the studied temperature range.

The first mass loss determined from the TG curve of the original hematite (Fig. 1f) is 0.95%, which is much less than the theoretical mass loss value of 3.44% as calculated from Eq. 1. This means that only a part of the hematite decomposes to magnetite, while most of the hematite is not yet decomposed. It was also widely reported that the reduction of α-Fe_2O_3 surfaces leads to the formation of Fe_3O_4 as determined by low-energy electron diffraction (LEED) and scanning tunneling microscopy (STM) studies. Annealing of iron oxides under selected oxygen partial pressures or high vacuum shifts the hematite–magnetite equilibrium toward formation of a phase stable under those conditions [25]. All these point to the relative stability and difficulty of decomposing hematite in the presence of argon. The small mass loss up to temperature of ~100 °C for all the investigated samples can be attributed to the surface physically adsorbed water.

In order to investigate the thermal stability of hematite in air, the original hematite samples were annealed at 450, 550, 650, and 750 °C, respectively. Simultaneous DSC–TG experiments were performed on these annealed samples. The thermal measurements of the annealed hematite samples are shown in Fig. 1b–e (DSC), g–j (TG).

The DSC curves of annealed hematite samples are similar to those of original hematite sample, with a broad peak and an uncompleted one (Fig. 1b–e). However, there are still some obvious differences. The DSC curves of annealed samples have a shoulder on the main exothermic peak, which indicates there is a possible intermediate step during the decomposition of hematite to nonstoichiometric magnetite. The decomposition reactions of the annealed hematite samples start at the same temperature as for original hematite, while these broad peaks culminate at much higher temperature. When hematite was annealed at 750 °C, this broad peak reached maximum at 377 °C with a shoulder at 554 °C, and culminates at 740 °C. This means that the annealing process in air increases the thermal stability of hematite in argon atmosphere. The increase of enthalpy with the increase in the annealing temperature of the annealed hematite in air is probably due to the intermediate step of decomposition.

The increase of thermal stability of hematite in argon atmosphere by increasing the annealing temperature of hematite in air can be confirmed by the TG curves of the annealed samples (Fig. 1g–j). The first mass loss curve of the annealed samples is not as sharp as that of original hematite; the overall values of the first mass loss decrease with the increase of annealing temperature. When hematite was annealed at 750 °C, this mass loss is only 0.23%, which is four times smaller than that of original hematite. No second mass loss was observed for this sample, which

is different from that of the hematite samples annealed at 450, 550, and 650 °C, respectively, possibly due to the increase in particle size at higher annealing temperature.

The mass loss from the annealed hematite samples also suggested that the observed mass loss from original hematite sample is not from chemically absorbed water or possible organic residue in the original hematite sample. The mass loss must be due to the decomposition of hematite under Ar atmosphere.

In order to investigate the effect of isothermal annealing process on the phase information of the annealed hematite samples, XRD experiments were performed. Figure 2 shows the XRD patterns of the original hematite and annealed hematite samples. It can be seen that the hematite is very stable when it is annealed in air, with typical pure hematite diffraction pattern in agreement with the pattern of JPCDS card No. 33-0664. The observation of mass loss of the annealed hematite samples under Ar atmosphere suggested the different thermal stabilities of hematite under different atmospheres. Figure 3 shows the average particle size of hematite samples as a function of annealing temperatures; the particle sizes of hematite samples were estimated by Scherrer equation using the strongest diffraction peak (104). The average particle size of the original hematite sample is ~47 nm, and it increased slightly when hematite was annealed below 650 °C. After being annealed at 750 °C, it has an average particle size of ~60 nm, this also confirmed our previous assumption that the abnormal DSC profile for this sample is from the different particle size. The changes in average particle sizes represent the crystallization of hematite when annealed under air atmosphere.

Although the hematite phase is stable under the annealing process in air, the lattice parameters *a* and *c* vary with the annealing temperature. Figure 4 shows the change of hematite lattice parameters *a* and *c* as a function of annealing temperature. It can be seen that the overall trends of *a* and *c* values are to decrease with the increase in the annealing temperature. It means that the annealing process causes the contraction of hematite unit cell. When the annealing temperature reaches 600 °C, the lattice parameters *a* and *c* level off, indicating the completion of the crystallization process. The DSC and TG curves, which show trends of increase in enthalpy and decrease in mass loss as a function of annealing temperature, also confirm that the annealing process in air affects the thermal stability of hematite in argon atmosphere.

In order to investigate the effect of smaller particle size on the thermal stability of hematite, samples of hematite were exposed to mechanochemical activation by high energy ball milling for 0–27 h. The particle size was found to decrease with the increase of the ball-milling time [25], with average size of 21.2 nm after 2 h of ball milling. After 8 h of ball milling, the average particle size of hematite was found to be 16.5 nm. No great change in the average hematite particle size was observed after long ball-milling time. The DSC and TG experiments were performed on those milled hematite samples.

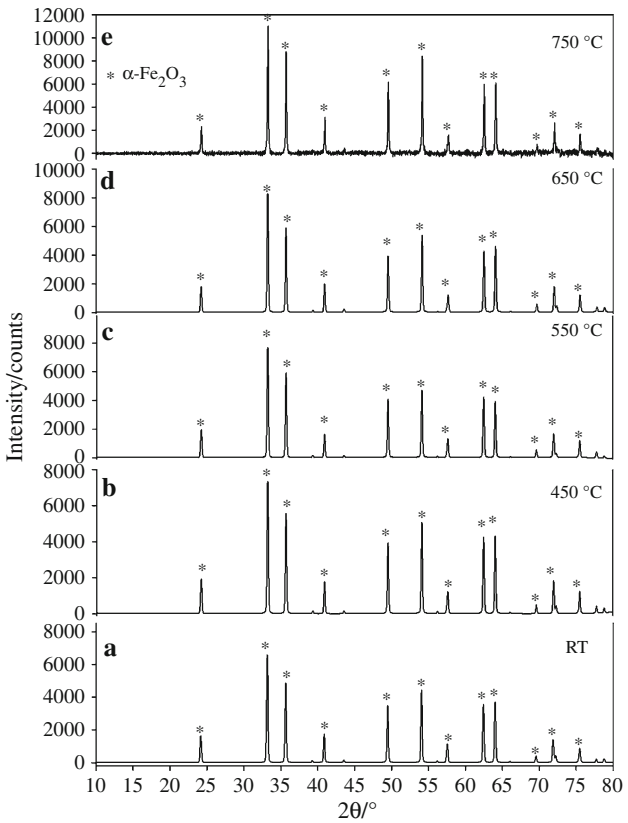

Fig. 2 XRD patterns of hematite samples annealed at *a* room temperature, *b* 450 °C, *c* 550 °C, *d* 650 °C, and *e* 750 °C

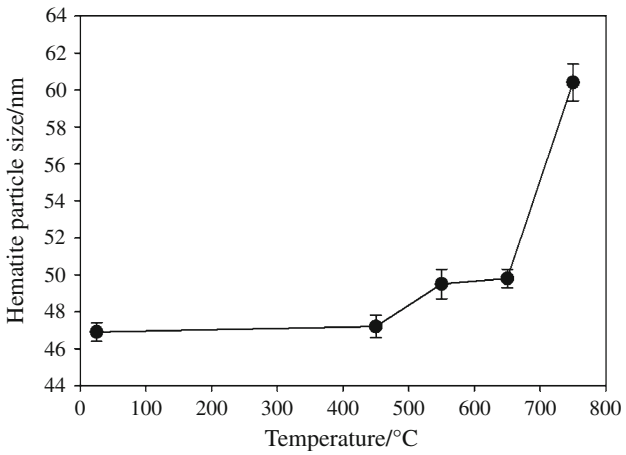

Fig. 3 Average particle size of hematite samples as a function of annealing temperatures

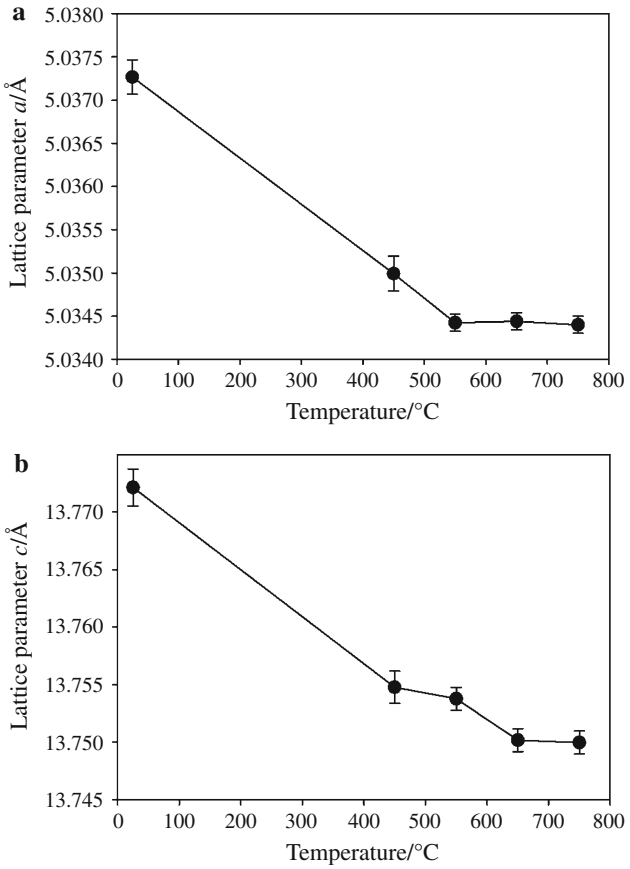

Fig. 4 Lattice parameters *a* and *c* of hematite samples as a function of annealing temperatures: **a** lattice parameter *a* and **b** lattice parameter *c*

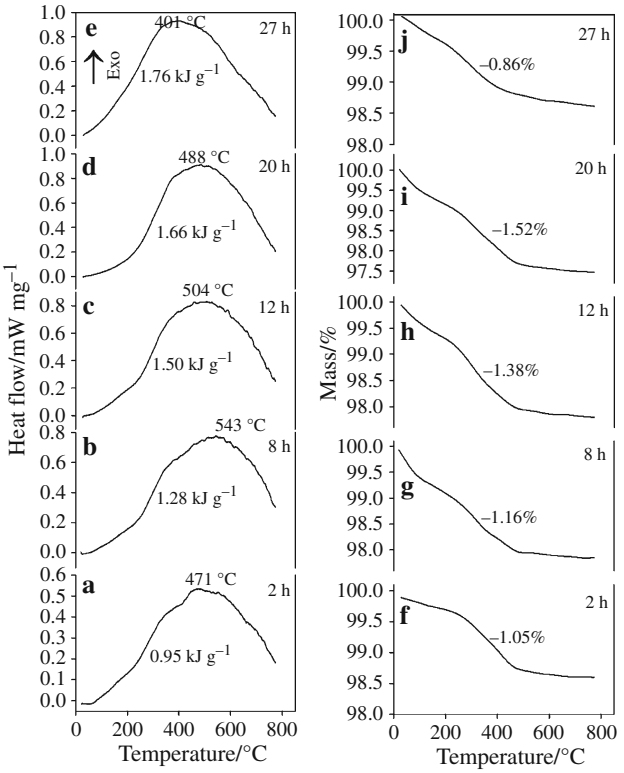

Fig. 5 DSC curves of hematite samples balled milled for *a* 2 h, *b* 8 h, *c* 12 h, *d* 20 h, and *e* 27 h and TG curves of hematite samples ball milled for *f* 2 h, *g* 8 h, *h* 12 h, *i* 20 h, and *j* 27 h

The DSC curves of hematite samples after different ball-milling time, Fig. 5a–e, show a broad exothermic peak with peak temperature from 400 to 500 °C, which is completely different from that of the original hematite sample (Fig. 1a), indicating the average particle size of hematite has an important effect on its thermal behavior, which is in agreement with DSC–TG results of the annealed hematite samples. The enthalpy associated with this broad peak increases with the decrease of particle sizes. This enthalpy value is due to the phase change in this temperature range and the crystallization of fine hematite particles during the DSC process, which releases energy as well. By analyzing the TG curves of these ball-milled hematite samples (Fig. 5f–j), it was found that the mass loss of ball-milled hematite starts at a much lower temperature than that of original hematite, but the final temperatures are almost the same. This indicates that the ball-milled hematite with smaller particle sizes is more likely to decompose into magnetite, which further confirmed the TG results that the annealed hematite samples with larger average particle size have smaller mass loss. However, no second mass loss was observed for all of the ball-milled hematite samples under 800 °C, which means that the particle size has a pronounced impact on the thermal behavior of hematite in argon gas. The broad peak is due to the thermal decomposition of hematite and the increase of the average particle size during heat treatment. It can also be seen that the mass loss increases with the increase in the ball-milling time, in other words, decreasing the particle size of starting hematite. This indicates that the hematite with a large particle size is more stable than that with small particle sizes. To the best of our knowledge, this study is the first evidence for the effect of particle size on the thermal behavior of nanoparticles.

The mass loss corresponding to hematite ball-milled for 27 h is less than that of hematite sample with shorter ball-milling time. This is due to the fact that the ball-milling process for 27 h caused part of hematite to convert to magnetite and the iron phase, as identified by Mössbauer spectrum measurement [23]. The lesser hematite in the starting materials for the DSC experiment causes the drop of mass loss percentage. Betancur et al. [26] studied the dynamics of transformation from hematite to magnetite by two ball-milling solid-state methods. One of the procedures involved a thermal treatment under H_2 (20%) and N_2 (80%) atmosphere at 375 °C, while the second method involved the ball milling to induce the transformation. The first

method indicated a well-behaved structural transformation for which highly stoichiometric Fe_3O_4 as a single phase was obtained after treatment for more than 12.5 min. A less stoichiometric magnetite in the case of ball-milled samples was obtained. Wiltowski et al. [27] and Piotrowski et al. [28] investigated the kinetics of hematite to wüstite reduction using thermogravimetric method in the temperature range of 700–900 °C. A reducing atmosphere composed of N_2 (90%), CO $(10 - x)$%, and H_2 (x%) was used with a flow rate of 30 mL/min. They found that the reduction of hematite is a surface-controlled process. However, once a thin layer of iron oxides with lower oxidation state is formed at the surface, it changes to diffusion control. In our case, the hematite could be reduced under inert atmosphere (Ar gas) by using the thermogravimetric method, and only part of hematite decomposed to iron oxides with the lower oxidation state.

Conclusions

Hematite is stable when it is annealed under air atmosphere. The lattice parameters a and c decrease with the annealing temperatures and level off when annealing temperature reaches 600 °C. The thermogravimetric behavior of the original and annealed hematite shows that the system is not stable when it is heated in inert argon atmosphere by means of a DSC–TG measurement, as hematite partially decomposes to lower oxidation state, such as magnetite or wüstite. The annealing process changed the decomposition mechanism of hematite, such that an intermediate step occurs, as shown by the increase of enthalpy value and the appearance of an extra exothermic peak around 550 °C.

Particle size has an important effect on the thermal stability of hematite, which is evidenced from both the ball-milled and isothermally annealed hematite samples. The DSC curves of ball-milled samples showed that the phase transformation was extended to higher temperature with larger enthalpy. On the other hand, the mass loss of ball-milled samples with smaller particle size starts at lower temperature than that of original hematite, and the mass loss percentage increases with the milling time.

Acknowledgements This study was supported by the National Science Foundation under grant number DMR-0854794.

References

1. Wang GX, Gou XL, Horvat J, Park J. Facile synthesis and characterization of iron oxide semiconductor nanowires for gas sensing application. J Phys Chem C. 2008;112:15220–5.
2. Raffaella B, Etienne S, Cinzia G, Fabia G, Mar GH, Miguel AG, Roberto C, Pantaleo DC. Colloidal semiconductor/magnetic heterostructures based on iron-oxide-functionalized brookite TiO_2 nanorods. Phys Chem Chem Phys. 2009;11:3680–91.
3. Winter G. Anorganic pigments: dispersed festkörper mit technisch verwertbaren optischen und magnetischen eigenschaften. Fortschr Miner. 1979;57:172–202.
4. Krishnamoorthy S, Rivas JA, Amiridis MD. Catalytic oxidation of 1,2-dichlorobenzene over supported transition metal oxides. J Catal. 2000;193:264–72.
5. Sorescu M, Diamandescu L, Tomescu A, Tarabasanu-Mihaila D, Teodorescu V. Structure and sensing properties of $0.1SnO_2$–$0.9Fe_2O_3$ system. Mater Chem Phys. 2008;107:127–31.
6. Laberty C, Navrotsky A. Energetics of stable and metastable low-temperature iron oxides and oxyhydroxides. Geochim Costmochim Acta. 1998;62:2905–13.
7. Greedan JE. Magnetic oxides. In: King RB, editor. Encyclopedia of inorganic chemistry. New York: Wiley; 1994.
8. Bernal JD, Dasgupta DR, Mackay AL. The oxides and hydroxides of iron and their structural inter-relationships. Clay Miner Bull. 1959;4:15–30.
9. Scholder R. Recent investigations on oxometallates and double oxides. Anges Chem. 1962;1:220–4.
10. Gump JR, Wagner WF, Schreyer JM. Preparation and analysis of barium ferrate (VI). Anal Chem. 1954;26:1957.
11. Ichida T. Mössbauer study of the thermal decomposition products of $BaFeO_4$. J Solid State Chem. 1973;7:308–15.
12. Withers RL, Bursill LA. Higher-order structural relationships between hematite and magnetite. J Appl Crystallogr. 1980;13:346–53.
13. Barbier A, Weiss W, Van Hove MA, Somorjai GA. Magnetite Fe_3O_4(111): surface structure by LEED crystallography and energetic. Surf Sci. 1994;302:259–79.
14. Gautier-Soyer M, Pollack M, Henriot M, Guittet MJ. The (1×2) reconstruction of the α-Fe_2O_3 $(\bar{1}012)$ surface. Surf Sci. 1996;352–354:112–6.
15. Fan HM, Yi JB, Yang Y, Kho KW, Tan HR, Shen ZX, Ding J, Sun XW, Olivo MC, Feng YP. Single-crystalline MFe_2O_4 nanotubes/nanorings synthesized by thermal transformation process for biological applications. ACS Nano. 2009;3:2798–808.
16. Navrotsky A, Mazeina L, Majzlan J. Size-driven structural and thermodynamic complexity in iron oxides. Science. 2008;319:1635–8.
17. Jozwiak W, Kaczmarek E, Maniecki TP, Ignaczak W, Maniukiewicz W. Reduction behavior of iron oxides in hydrogen and carbon monoxide atmospheres. Appl Catal A. 2007;326:17–27.
18. Misono M, Sakata K, Ueda F, Nozawa Y, Yoneda Y. Catalytic properties of iron oxide III. Oxidative dehydrogenation of butenes over iron oxide catalysts. Bull Chem Soc Jpn. 1980;53:648–52.
19. Holleman AF, Wiberg E. Inorganic chemistry. San Diego: Academic Press; 2001.
20. Sorescu M, Xu TH, Diamandescu L. Synthesis and characterization of $x TiO_2 \cdot (1 - x)\alpha$-$Fe_2O_3$ magnetic ceramic nanostructure system. Mater Character. 2010;61:1103–18.
21. Sorescu M, Xu TH. The effect of ball-milling on the thermal behavior of anatase doped hematite systems. J Therm Anal Calorim. 2010. doi:10.1007/s10973-010-1016-1.
22. Snow CL, Lee CR, Shi Q, Boerio-Goates J, Woodfield BF. Size-dependence of the heat capacity and thermodynamic properties of hematite (α-Fe_2O_3). J Chem Thermodyn. 2010;42:1142–51.
23. Sorescu M, Diamandescu L. Mechanochemical and magneto-mechanical synthesis of hematite nanoparticles. Hyperfine Interact. 2010;196:349–58.
24. Lin CR, Chiang RK, Cheng CJ, Lai HY, Lyubutin IS, Alkaev EA. Preparation of magnetite nanoparticles by thermal decomposition

of hematite powder in the presence of organic solvent. In: Pappas DP, editor. Nanoscale magnetics and device applications. Mater Res Soc Symp Proc; 2007. 998E: 0998-J08-05.
25. Fellows RA, Lennie AR, Raza H, Pang CL, Thornton G, Vaughan DJ. Fe_3O_4 formation on a reduced α-Fe_2O_3 ($11\bar{2}3$) substrate: a low-energy electron diffraction and scanning tunneling microscopy study. Surf Sci. 2000;445:11–7.
26. Betancur JD, Restrepo J, Palacio CA. Thermally driven and ball-milled hematite to magnetite transformation. Hyperfine Interact. 2003;148:163–75.
27. Wiltowski T, Piotrowski K, Lorethova H, Stonawski L, Mondal K, Lalvani SB. Neural network modeling of iron oxide reduction kinetics. Chem Eng Proc. 2005;44:775–83.
28. Piotrowski K, Mondal K, Lorethova H, Stonawski L, Szymanski T, Wiltowski T. Effect of gas composition on the kinetics of iron oxide reduction in a hydrogen process. Int J Hydrogen Energy. 2005;30:1543–54.